

Three-dimensional simulation of wave-induced circulation: Comparison of three radiation stress formulations

Y. Peter Sheng¹ and Tianyi Liu¹

Received 24 October 2010; revised 9 January 2011; accepted 25 February 2011; published 27 May 2011.

[1] A three-dimensional current-wave modeling system, Curvilinear-grid Hydrodynamics 3D (CH3D)-Simulating Waves Nearshore (SWAN), has been used to simulate wave-induced circulation and compare the performances of three radiation stress (RS) formulations: two depth-dependent formulations (M08 by Mellor (2008) and X04 by Xia et al. (2004)) and one depth-independent formulation (LHS by Longuet-Higgins and Stewart (1964)). While all are based on linear wave theory, LHS uses the vertically integrated equations of motion, and M08 and X04 consider the three-dimensional equations of motion. Results of CH3D-SWAN with three RS formulations are compared with steady state wave setup, observed data in an undertow experiment by Ting and Kirby (1994) (TK94), and observed data in a laboratory fringing reef. All three RS formulations reproduce the analytical solution of wave setup very well. Simulated wave-induced currents and turbulence for TK94 are the best when M08 is used and worst when X04 is used, apparently due to the errors in the X04 formulation. All three RS formulations give good simulation of wave setup in the fringing reef. Wave-induced currents in the fringing reef simulated by the three RS formulations are quite different: M08 produces a single large clockwise gyre in the x - z plane, LHS produces a weaker gyre, and X04 produces a clockwise gyre plus a counterclockwise gyre inside the surf zone. Using the CH3D-Storm Surge Modeling System and M08, storm surge and currents in the Outer Banks and Chesapeake Bay during Hurricane Isabel are simulated. Compared to the earlier simulation obtained with the LHS, M08 produces similar storm surge but slightly improved the wave-induced currents.

Citation: Sheng, Y. P., and T. Liu (2011), Three-dimensional simulation of wave-induced circulation: Comparison of three radiation stress formulations, *J. Geophys. Res.*, 116, C05021, doi:10.1029/2010JC006765.

1. Introduction

[2] Wave current interaction is of great importance to the nearshore hydrodynamics. Wave-induced setup is a rise of the water elevation above the still sea level (mean sea level in the absence of waves), and the wave-induced currents are essential to understanding bottom sediment transport and shoreline changes. Momentum flux directed shoreward by water waves, commonly referred to as radiation stress (RS), has been studied by Longuet-Higgins and Stewart [1962, 1964], and development of this concept led to a greater understanding of wave-induced circulation [Longuet-Higgins, 1970a, 1970b; Svendsen 1984a, 1984b; Stive and Wind, 1986].

[3] Zhang and Li [1996] and Roland et al. [2009] applied 2DH (two-dimensional horizontal) circulation models with the vertically integrated radiation stress of Longuet-Higgins and Stewart [1964], to examine the effects of wave on storm surge simulations. However, the vertical structures of cur-

rents cannot be obtained from these 2DH simulations. Using 2DH circulation models and LHS, vertical variations in horizontal velocities are introduced by solving the time averaged and vertically integrated continuity and momentum equations derived for nonuniform currents which are divided into a wave component and a current component [Dongeren et al., 1994; Haas et al., 2003; Wang et al., 2008]. These models are often referred to as quasi 3-D models.

[4] Recent studies have used 3-D circulation models and LHS to study wave-induced circulation [e.g., Xie et al., 2001; Sheng and Alymov, 2002; Sheng et al., 2010a, 2010b]. These studies yield vertically varying currents and eddy coefficients and reasonably accurate wave-induced circulation. However, Mellor [2003, 2008] and Xia et al. [2004] questioned the accuracy of the vertically uniform LHS, and developed depth-dependent RS formulations: M03 [Mellor, 2003], X04 [Xia et al., 2004], and M08 [Mellor, 2008]. While all three formulations are based on linear wave theory, X04 is obtained with a simplistic approach which invokes the small amplitude approximation in part of the LHS to allow interchanging of the time integration and vertical integration to develop a depth-dependent RS, while M03 and M08 both consider the wave effects on

¹Civil and Coastal Engineering Department, University of Florida, Gainesville, Florida, USA.

three-dimensional equations of motion. However, M03 was found to contain error [Ardhuin *et al.*, 2008b] and M08 requires some additional fixes by G. L. Mellor (The depth-dependent current and wave interaction equations: An addendum, unpublished manuscript, 2009), while X04 yields questionable results due to its simplifying approximations. Nevertheless, when vertically integrated, both X04 and M08 produce the same vertically integrated RS as the LHS.

[5] Haas and Warner [2009] used the quasi 3-D SHOR-ECIRC (with LHS) and the 3-D Regional Ocean Modeling System (ROMS) [Song and Haidvogel, 1994] (with M03) to simulate simple analytical and laboratory wave-induced circulation, and obtained qualitatively similar results. Using Princeton Ocean Model (POM)-[Mellor, 1996] Simulating Waves Nearshore (SWAN) [Booij *et al.*, 1999] and X04, Xie *et al.* [2008] studied the effects of wave-current interaction on circulation, while Liu and Xie [2009] studied the effects of wave-current-surge interaction on wave. However, the validity and accuracy of the depth-dependent radiation stresses, X04 and M08, have never been critically assessed by comparing simulated versus analytical or observed wave-induced circulation (e.g., wave setup, wave-induced currents).

[6] Besides the development of the radiation stress concept, there are also other kinds of theories to represent wave effects in wave driven circulations. The formulation of vortex force, which is a coupling of the vorticity in a current and mean wave momentum, was derived to represent the wave averaged forcing on circulation [Craik and Leibovich, 1976]. Taking account of the asymptotic scaling, McWilliams *et al.* [2004] provided a vertically varying vortex force form, which was implemented into the three-dimensional circulation model ROMS by Uchiyama *et al.* [2010]. Newberger and Allen [2007] applied a vortex force formulation to three-dimensional wave-averaged mean circulation in the surf zone, and studied the wave current interactions in shallow waters. The generalized Lagrangian mean (GLM) method, which is able to split the mean and oscillating motions, was initially developed by Andrews and McIntyre [1978] to describe wave current interactions. Groeneweg [1999] derived the three-dimensional GLM equations for the combined wave-current motion, and used a one-dimensional model to study nonbreaking long-crested waves on a current. Ardhuin *et al.* [2008a] developed the three-dimensional GLM wave-averaged momentum equations to second order in wave slope, and strong and sheared mean currents with limited curvature in the current profile were also accounted.

[7] In this study, we aim to give a critical assessment on the validity and accuracy of the three RS formulations: LHS, X04, and M08 for simulating wave-induced circulation in coastal waters. LHS and the depth-dependent X04 and M08 formulations are incorporated into a three-dimensional current-wave modeling system, Curvilinear-grid Hydrodynamics 3D (CH3D)-SWAN, which is the cornerstone of the CH3D-Storm Surge Modeling System (SSMS) [Sheng *et al.*, 2010a, 2010b]. CH3D-SWAN consists of a three-dimensional hydrodynamic model CH3D [Sheng, 1986] and a wave model SWAN [Booij *et al.*, 1999]. By comparing simulated versus analytical and observed wave-induced circulation, the performances of the two depth-dependent RS formulations X04 and M08 and the depth-independent LHS radiation stress are assessed.

[8] Section 2 of the paper describes the CH3D-SWAN model and the three RS formulations. Section 3 presents the results of four test simulations using CH3D-SWAN. Conclusions are given in section 4.

2. Methodology

2.1. A Three-Dimensional Circulation Model: CH3D

[9] CH3D, a three-dimensional circulation model originally developed by Sheng [1986, 1987], has been successfully applied to simulate the estuarine, coastal and riverine circulation driven by tide, wind and density gradients in various water bodies [e.g., Sheng *et al.*, 2010a, 2010b]. The model uses a boundary fitted nonorthogonal curvilinear grid in the horizontal directions to resolve the complex shoreline and geometry, and a terrain-following σ grid in the vertical direction. The model uses a Smagorinski-type horizontal diffusion coefficient, a robust turbulence closure model [Sheng and Villaret, 1989] for the vertical mixing, and highly accurate advective schemes QUICKEST [Leonard, 1979] and Ultimate QUICKEST [Leonard, 1991].

[10] The equations of motion for CH3D, in rectangular coordinates, are [Sheng *et al.*, 2010a]

$$\frac{\partial u}{\partial x} + \frac{\partial v}{\partial y} + \frac{\partial w}{\partial z} = 0, \quad (1)$$

$$\begin{aligned} \frac{\partial u}{\partial t} + \frac{\partial uu}{\partial x} + \frac{\partial uv}{\partial y} + \frac{\partial uw}{\partial z} + \frac{1}{\rho_w} \frac{\partial S_{xx}}{\partial x} + \frac{1}{\rho_w} \frac{\partial S_{xy}}{\partial y} = -g \frac{\partial \zeta}{\partial x} - \frac{1}{\rho_w} \frac{\partial P_a}{\partial x} \\ - \frac{g}{\rho_w} \frac{\partial}{\partial x} \int_z^\zeta \rho dz + f v + A_H \left(\frac{\partial^2 u}{\partial x^2} + \frac{\partial^2 u}{\partial y^2} \right) + \frac{\partial}{\partial z} \left(A_V \frac{\partial u}{\partial z} \right), \end{aligned} \quad (2)$$

$$\begin{aligned} \frac{\partial v}{\partial t} + \frac{\partial vu}{\partial x} + \frac{\partial vv}{\partial y} + \frac{\partial vw}{\partial z} + \frac{1}{\rho_w} \frac{\partial S_{yx}}{\partial x} + \frac{1}{\rho_w} \frac{\partial S_{yy}}{\partial y} = -g \frac{\partial \zeta}{\partial y} - \frac{1}{\rho_w} \frac{\partial P_a}{\partial y} \\ - \frac{g}{\rho_w} \frac{\partial}{\partial y} \int_z^\zeta \rho dz - f u + A_H \left(\frac{\partial^2 v}{\partial x^2} + \frac{\partial^2 v}{\partial y^2} \right) + \frac{\partial}{\partial z} \left(A_V \frac{\partial v}{\partial z} \right). \end{aligned} \quad (3)$$

The hydrostatic approximation states

$$\frac{\partial p}{\partial z} = -\rho g, \quad (4)$$

where $u(x,y,z,t)$, $v(x,y,z,t)$, and $w(x,y,z,t)$ are the wave-averaged velocity vector components [LT^{-1}] in x , y , and z directions, respectively; t is time [T]; $\zeta(x,y,t)$ is the free surface elevation [L]; g is the acceleration of gravity [L^{-2}T^2]; ρ is the water density; ρ_0 is the reference density (1 g/cm^3); A_H and A_V are the horizontal and vertical turbulent eddy coefficients, respectively [L^2T^{-1}]; and f is the Coriolis component [T^{-1}]. S_{xx} , S_{xy} , S_{yx} and S_{yy} are radiation stress terms. P_a is atmospheric pressure. Here ρ is determined by an equation of state which relates ρ to temperature and salinity.

[11] The CH3D model uses boundary-fitted non-orthogonal coordinates in the horizontal directions and a terrain-following σ coordinate in the vertical direction. The horizontal momentum equations, in the curvilinear co-

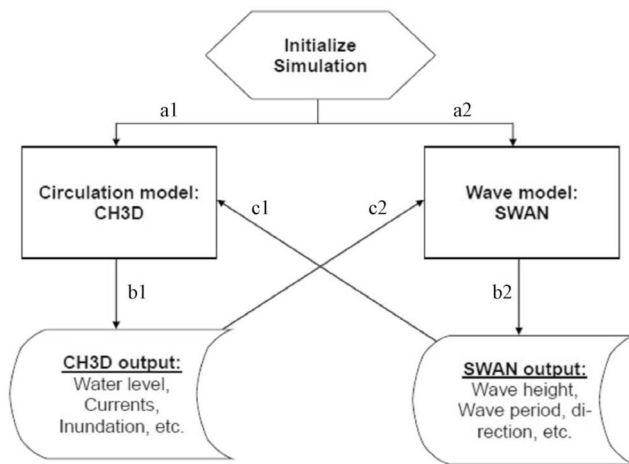


Figure 1. The coupling process between CH3D and SWAN; arrows a, b, and c are the time sequence in the coupling process and each of them includes two independent processes (1 and 2).

ordinates, are written in terms of the contravariant velocity vectors. As pointed out by *Sheng et al.* [2010a], the wave-averaged equations (1)–(4) are valid for two regions: the region between the free surface (mean sea level) and the wave trough, as well as the region between the wave trough and the bottom. In the region above the wave trough, the wave-averaged horizontal currents include the mean currents and the Stokes drift, while the radiation stress includes the vertically uniform radiation stress according to *Longuet-Higgins and Stewart* [1964] plus that due to the surface roller [*Svendsen*, 1984b; *Haas and Svendsen*, 2000]. Below the wave trough, the Stokes drift is zero, while the radiation stress does not have the surface roller contribution.

[12] The governing equations, boundary conditions, and representation of various wave effects for CH3D, in the horizontally boundary-fitted nonorthogonal curvilinear coordinates and vertically terrain-following coordinate are given in Appendix A of *Sheng et al.* [2010a].

2.2. A Shallow Water Wave Model: SWAN

[13] The SWAN model [*Booij et al.*, 1999] is a third-generation wave model which computes random, short-crested waves in coastal regions and inland waters. It accounts for wave propagation in time and space, shoaling, refraction due to current and depth, frequency shifting due to currents and nonstationary depth, wave generation by wind, bottom friction, depth-induced breaking, and transmission through and reflection from obstacles. The model predicts a 2-D wavefield on the grid points, and the waves are described with the two-dimensional wave action density spectrum $N(\sigma, \theta)$ equal to the energy density divided by the relative frequency: $N(\sigma, \theta) = E(\sigma, \theta)/\sigma$.

[14] The evolution of the wave spectrum is described by the spectral action balance equation

$$\frac{\partial}{\partial t} N + \frac{\partial}{\partial x} c_x N + \frac{\partial}{\partial y} c_y N + \frac{\partial}{\partial \sigma} c_\sigma N + \frac{\partial}{\partial \theta} c_\theta N = \frac{S}{\sigma}. \quad (5)$$

The first term on the left hand side of (5) represents the local rate of change of action density in time, while the second

and third terms represent propagation of action in geographical space (with propagation velocities c_x and c_y) in x and y space, respectively. The fourth term represents shifting of the relative frequency due to variations in depths and currents (with propagation velocity c_σ in σ space). The fifth term represents depth-induced and current-induced refraction (with propagation velocity c_θ in θ space). The expressions for these propagation speeds are taken from linear wave theory. The term $S (= S(\sigma, \theta))$ at the right hand side of the action balance equation is the source term in terms of energy density representing the effects of generation, dissipation and nonlinear wave-wave interactions, etc.

2.3. The Coupling Between CH3D and SWAN

[15] The circulation and wave models, CH3D and SWAN, are dynamically coupled. SWAN provides the wavefield information (wave height, period, and directions) at each grid cell which are used to estimate the radiation stress terms in the momentum equations in CH3D, as well as the wave enhanced bottom friction and eddy viscosity. Wave setup and wave-induced currents are computed by CH3D, while the water elevation which includes wave setup may change the total water depth and hence altering the wave propagation process. The currents simulated by CH3D would affect the wave propagation by inducing wave refraction. Therefore, the coupled CH3D-SWAN allows the wave and current to interact with each other. The coupling process of CH3D and SWAN is shown in Figure 1.

2.4. Three Formulations of Radiation Stresses: LHS, X04, and M08

2.4.1. The Vertically Integrated Radiation Stress and Mass Transport by *Longuet-Higgins and Stewart* [1964]: LHS

[16] The vertically integrated LHS radiation stress formulation, which is the time integration (over a wave period) of the vertical integration of the horizontal momentum, can successfully explain the wave setup and setdown inside and outside the surf zone, rip current and longshore currents. The expression for the vertically integrated radiation stresses are

$$S_{xx} = E \left[n(\cos^2 \theta + 1) - \frac{1}{2} \right], \quad (6)$$

$$S_{yy} = E \left[n(\sin^2 \theta + 1) - \frac{1}{2} \right], \quad (7)$$

$$S_{xy} = S_{yx} = \frac{E}{2} n \sin 2\theta, \quad (8)$$

where E is the wave energy, θ is the angle of wave propagation to the onshore direction and n is the ratio of group velocity to wave celerity, $n = (1 + 2kh/\sinh 2kh)/2$.

[17] The wave-induced mass transport is given by *Svendsen* [1984b] as

$$Q_{w\alpha} = B_0 \frac{gH^2}{c} \frac{k_\alpha}{k}, \quad (9)$$

where α is the horizontal coordinate, H is the wave height, c is the wave phase speed, k is the wave number, B_0 is

waveshape factor which is defined as, $B_0 = (1 + G)/16$, where $G = 2kh/\sinh(2kh)$.

[18] The surface roller term developed by *Svendsen* [1984b] plays an important role in mass, momentum and energy balance in the surf zone. The roller represents an increase in radiation stress which can be written as [Svendsen, 1984b]

$$S'_m = 0.9 \frac{h}{L} \rho g H_b^2 \quad (10)$$

and added to the region between the mean water level and wave trough. In CH3D, the criteria used to determine wave breaking is based on the ratio of significant wave height to water depth, $\gamma = H_{\text{sig}}/D$, where H_{sig} is the significant wave height and D is the total water depth. In the current study, breaking occurs when the coefficient is 0.78, a default in SWAN.

[19] The wave-induced mass transport inside the surf zone is

$$Q_{w\alpha} = \frac{gH^2}{c} \frac{c^2}{gh} \left(B_0 + \frac{A}{H^2} \frac{h}{L} \right) \frac{k_\alpha}{k}, \quad (11)$$

where L is the wavelength and A is the area for the surface roller of breaking waves, $A = 0.06HL$ [Okayasu *et al.*, 1988].

2.4.2. The Depth-Dependent Radiation Stress

Formulation by *Xia et al.* [2004]: X04

[20] *Xia et al.* [2004] developed a vertically varying RS formulation based on linear wave theory starting from the definition of radiation stress by LHS. For example, considering $\theta = 0$ in equations (6)–(8), the LHS radiation stress is

$$S_{xx} = \overline{\int_{-h}^{\zeta} (p + \rho u^2) dz} - \int_{-h}^0 p_0 dz, \quad (12)$$

where ζ is the free surface induced by waves; h is the depth; p_0 is the hydrostatic pressure in the absence of waves, and equals to $-\rho gz$. Equation (12) represents the difference between the total flux of horizontal momentum due to waves and the mean flux in the absence of the waves, following LHS.

[21] To derive depth-dependent RS, X04 used the terrain following coordinate transformation, $\sigma = (z - \zeta)/(h + \zeta)$, for the first term on the RHS of equation (12), but used an approximate form of coordinate transformation, $\sigma = z/h$, for the second term on the RHS of equation (12), and obtained

$$S_{xx} = \overline{\int_{-1}^0 (p + \rho u^2)(\zeta + h) d\sigma} - \int_{-1}^0 \rho g \sigma h^2 d\sigma. \quad (13)$$

Therefore, the coordinate transformations for the two terms on the RHS of equation (12) are inconsistent, and both terms in equation (13) are calculated from the bottom to the free surface, which is inconsistent with the definition of radiation stress in LHS, i.e., equation (12). By assuming $\sigma = z/h$, the second term of equation (13) has a different physical meaning than the second term of equation (12), and the σ values in the first and second terms are actually at different vertical locations. Hence the depth-dependent RS derived by

X04 contains errors, although the erroneous equation (13) enabled Xia to interchange the order of the time integration and the vertical integration to produce a depth-dependent RS. In addition, the horizontal gradients in the transformed coordinate system are simplified by assuming negligible bottom slope. The small amplitude assumption ($a \ll L$, a is the wave amplitude; L is the wavelength) is applied and all terms of higher order than ka are neglected. Therefore, because of the numerous approximations in Xia's derivation, the ensuing X04 formulation is erroneous, as will be evidenced by our test results presented later in the paper. We include X04 formulation in this study because it is used by several studies [e.g., *Xie et al.*, 2008; *Liu and Xie*, 2009].

[22] After exchanging the time integration with the vertical integration, the depth-dependent radiation stress X04 is found to be

$$S_{xx}(z) = E \frac{k}{\sinh 2kh} [\cosh 2k(z+h) + 1] \cos^2 \theta - E \frac{k}{\sinh 2kh} \cdot [\cosh 2k(z+h) - 1] - \frac{Ez}{D^2} + E \frac{k(z+h) \sinh k(z+h)}{h \cosh kh} - \frac{E}{D} \left[1 - \frac{\cosh k(z+h)}{\cosh kh} \right], \quad (14)$$

$$S_{yy}(z) = E \frac{k}{\sinh 2kh} [\cosh 2k(z+h) + 1] \sin^2 \theta - E \frac{k}{\sinh 2kh} \cdot [\cosh 2k(z+h) - 1] - \frac{Ez}{D^2} + E \frac{k(z+h) \sinh k(z+h)}{h \cosh kh} - \frac{E}{D} \left[1 - \frac{\cosh k(z+h)}{\cosh kh} \right], \quad (15)$$

$$S_{xy}(z) = E \frac{k}{\sinh 2kh} [\cosh 2k(z+h) + 1] \sin \theta \cos \theta, \quad (16)$$

$$S_{yx}(z) = S_{xy}(z), \quad (17)$$

where E is the wave energy, k is the wave number, h is the water depth. Here θ is the wave angle to the x coordinate.

[23] While Xia's formulation produced reasonable wave setup simulation, there has not been any direct validation of the simulated wave-induced currents. The simulated wave-induced circulation in a laboratory flume by *Xia et al.* [2004] shows shoreward bottom currents, instead of the seaward undertow, inside the surf zone. The vertical profile of X04 is shown in Figure 2 for deep ($kD = 8.0570$) and shallow ($kD = 0.2877$) waters, where the wave height is 0.5 m, the water depth is 2 m, and the wave propagates at an angle of 30° to the shore normal axis. For shallow water, the wave period is 10 s, while for deep water, the wave period is 1 s. Vertical profile of S_{xx} and S_{yy} show noticeable radiation stresses in the lower column of relatively deep (large kD) water, as shown in Figure 2. These radiation stresses in the lower column of relatively deep water are counterintuitive and apparently due to errors in X04 which result from the previously mentioned simplifying approximations.

2.4.3. The Depth-Dependent Radiation Stress by *Mellor* [2008]: M08

[24] *Mellor* [2008] developed a depth-dependent radiation stress formulation, M08, by rigorously deriving the three-dimensional continuity and momentum equations while

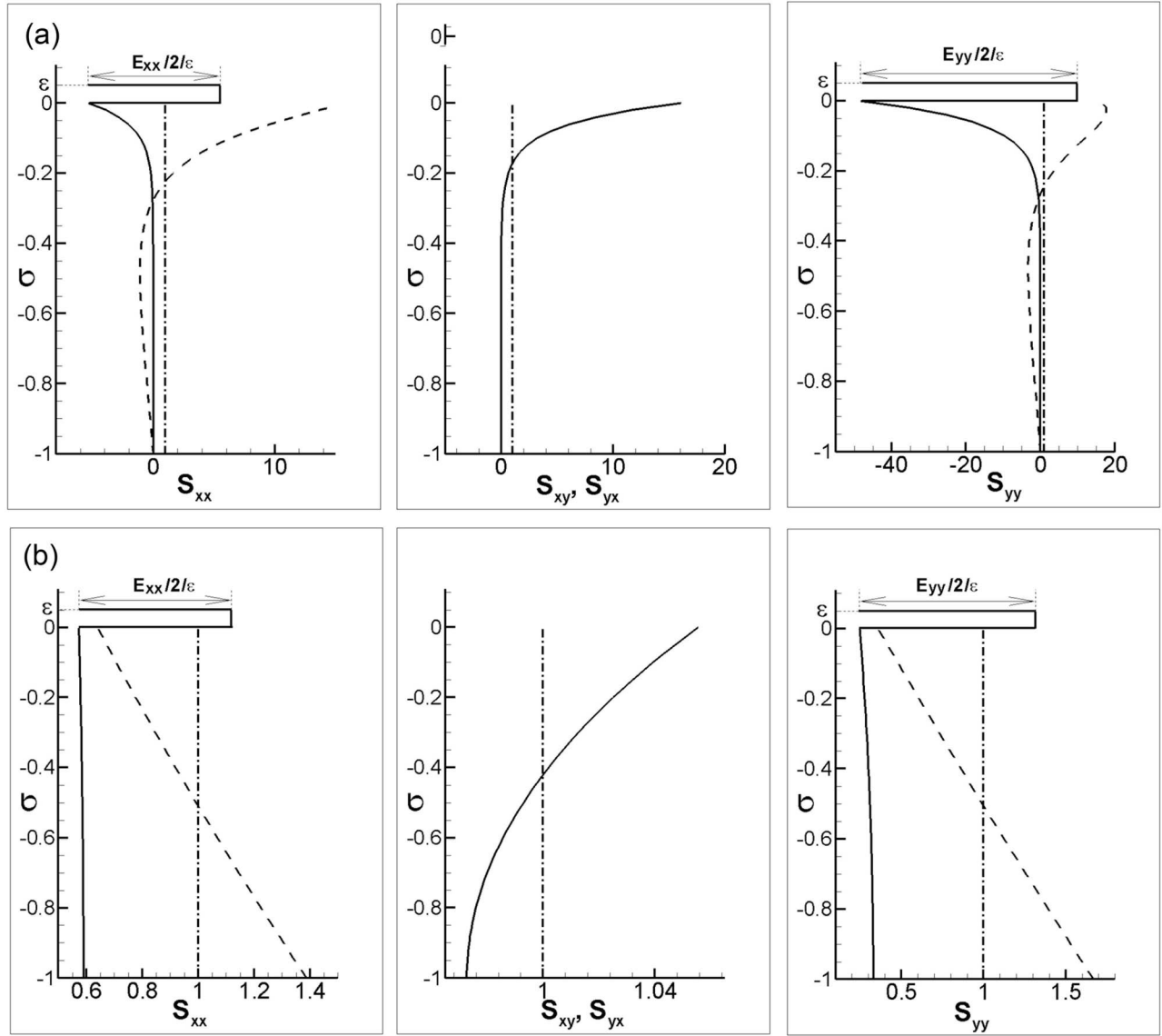


Figure 2. Distribution of dimensionless M08 (solid line), X04 (dashed line) and LHS (dash dot) in (a) deep water and (b) shallow water. Here ε is an infinitesimal distance above the mean water level, indicating the Dirac delta function E_D . Radiation stresses (M08, X04, LHS) are nondimensionalized by the LHS RS, E_{xx} is the wave energy E nondimensionalized by the LHS RS S_{xx} , and E_{yy} is the wave energy E nondimensionalized by the LHS RS S_{yy} .

including linear waves. While the earlier theory by Mellor [2003] (M03) contains error [Ardhuin *et al.*, 2008b] and do not produce the RS of LHS when vertically integrated, the vertically integrated form of M08 is consistent with LHS. M08 used the z coordinate but M03 used the vertically stretched σ coordinate. While the M08 derivation is also based on linear wave theory which works well for deep water, and assumes small ka values and small bottom slope, it does not contain as many simplifying assumptions as X04.

[25] The depth-dependent radiation stress by Mellor [2008] is

$$S_{\alpha\beta} = kE \left(\frac{k_\alpha k_\beta}{k^2} F_{CS} F_{CC} - \delta_{\alpha\beta} F_{SC} F_{SS} \right) + \delta_{\alpha\beta} E_D, \quad (18)$$

$$F_{SS} = \frac{\sinh k(z+h)}{\sinh kD}, \quad (19a)$$

$$F_{CS} = \frac{\cosh k(z+h)}{\sinh kD}, \quad (19b)$$

$$F_{SC} = \frac{\sinh k(z+h)}{\cosh kD}, \quad (19c)$$

$$F_{CC} = \frac{\cosh k(z+h)}{\cosh kD}, \quad (19d)$$

where α, β are horizontal coordinates, k is the wave number, E is wave energy, E_D is a modified Dirac delta function, and is defined according to Mellor [2008] as

$$E_D = 0 \text{ if } z \neq \zeta \text{ and } \int_{-h}^{\zeta+} E_D dz = \frac{E}{2}. \quad (20)$$

In shallow water the $E/2$ term is very large and has a profound impact. The physical significance of this term is explained here. In the wave-induced circulation simulation, the radiation stress terms dominate and are much larger than the other terms in the equations of motion. In the radiation stress terms, $E/2$ is large for shallow water (Figure 2). The

rent data. In relatively deep (large kD) water, as expected, M08 shows little radiation stress in the lower column, as shown in Figure 2.

[29] Feddersen [2004] compared the exact radiation stresses calculated from the field observed frequency directional wave spectrum with that calculated based on narrow-banded approximation, and found that the narrow-banded approximation overestimates the true radiation stresses. However, the formulation in equation (18) was derived for a monochromatic wave, so the frequency directional wave spectrum is needed to more accurately estimate the M08 RS. For random waves, equation (18) would become [Battjes, 1972]

$$S_{\alpha\beta} = \int_0^\infty \int_{-\pi}^\pi \left\{ k(f)E(f, \theta) \left[\frac{k_\alpha(f)k_\beta(f)}{k(f)^2} F_{CS}F_{CC} - \delta_{\alpha\beta}F_{SC}F_{SS} \right] + \delta_{\alpha\beta}E_D(f, \theta) \right\} d\theta df, \quad (23)$$

$E/2$ term comes from the pressure in the region between the wave crest and mean water level.

[26] In LHS, the integrated radiation stress is divided into three terms: $S_{xx} = S_{xx}^1 + S_{xx}^2 + S_{xx}^3$, where the last term is the $E/2$ term: $E/2 = S_{xx}^3 = \int_0^{\bar{\eta}} pdz$. M08 kept the original S_{xx}^3 term, but developed the S_{xx}^1 and S_{xx}^2 terms into 3-D. In shallow water, the term S_{xx}^3 is large which indicates that significant pressure between the wave crest and mean water level contributes to increased momentum flux. Recent experimental study [Gemrich, 2010] found that dissipation rates within nonbreaking wave crests are on average 3 times larger than values found at the same distance to the free surface but within the wave trough region. This ratio increases to 18 times for periods with frequent wave breaking.

[27] Mellor (unpublished manuscript, 2009) provided additional information on the boundary conditions for 3-D wave-current model

Continuity Equations

$$w = \frac{\partial \zeta}{\partial t} + u_\beta \frac{\partial \zeta}{\partial x_\beta}, \quad z = \zeta, \quad (21a)$$

$$w = -u_\beta \frac{\partial h}{\partial x_\beta}, \quad z = -h, \quad (21b)$$

Momentum Equation

$$wu_\alpha = \frac{\partial \zeta}{\partial t} u_\alpha + (u_\alpha u_\beta + \overline{\tilde{u}_\alpha \tilde{u}_\beta}) \frac{\partial \zeta}{\partial x_\beta}, \quad z = \zeta, \quad (22a)$$

$$wu_\alpha = -(u_\alpha u_\beta + \overline{\tilde{u}_\alpha \tilde{u}_\beta}) \frac{\partial h}{\partial x_\beta}, \quad z = -h, \quad (22b)$$

where $(\tilde{u}_\alpha, \tilde{w})$ is the linear wave velocity components [Mellor, 2008, equations (1b) and (1c)]; (u_α, w) are the phase averaged velocities [Mellor, 2008, equations (11a) and (11b)]; h is the water depth; the overbar indicates phase averaging.

[28] While Mellor's formulation makes fewer approximations and appears more rigorous than that of Xia *et al.* [2004], it has not been validated with wave-induced cur-

rent data. In relatively deep (large kD) water, as expected, M08 shows little radiation stress in the lower column, as shown in Figure 2.

2.5. Vertical Profile of the X04 and M08 Depth-Dependent Radiation Stresses

[30] The vertical profiles of the radiation stresses according to X04 and M08 are shown in Figure 2, and the wave conditions are given in section 2.4.2.

[31] In deep water, X04 shows some radiation stress (S_{xx}, S_{yy}) near the bottom, which is questionable since the wave effects near the bottom should be close to 0. In shallow water, M08 shows very slight variation in the water column, while X04 indicates an increase of wave effects from the surface to the bottom, which is counterintuitive and problematic. These raise questions about the validity and accuracy of X04 for simulating wave-induced circulation, while M08 appears to be more reasonable. In the following, we will compare the performance of X04 and M08 for simulating wave-induced circulation.

3. Test Simulations

[32] Using the coupled CH3D-SWAN and the three RS formulations, we compared the simulated results for an analytical solution of wave setup, a laboratory experiment on undertow, and a laboratory experiment of a fringing reef. All three RS formulations are incorporated into the curvilinear coordinates of CH3D. For simplicity, however, the RS formulations in the curvilinear coordinates will not be shown here.

3.1. Steady State Wave Setup: An Analytical Solution

[33] Wave setup generally occurs in the surf zone. As the waves shoal and break on a beach, they produce excess momentum flux in the shoreward direction. At the steady state, the shoreward decrease of the radiation stress is balanced by a shoreward increase in the water level. This raises the water surface elevation within the surf zone to be higher than the still water level and produces a setup. The balance between pressure gradient and shoreward increase of radiation stress in wave shoaling produce a wave setdown. The

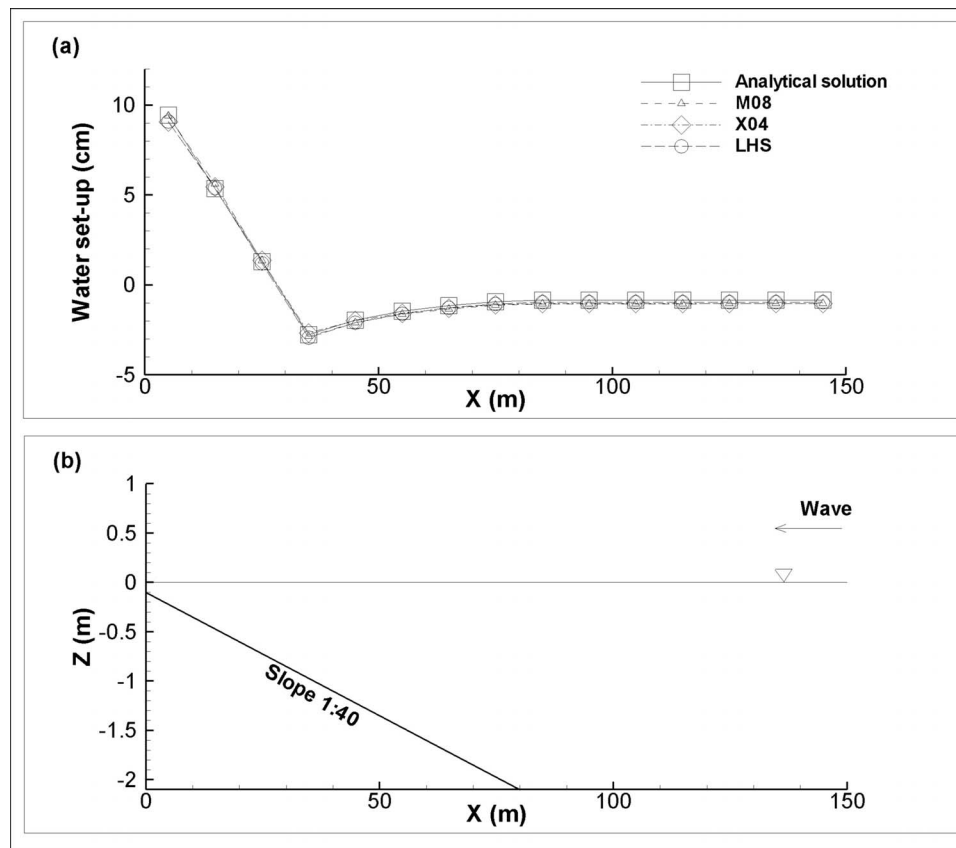


Figure 3. (a) The comparison between analytical and numerical solution for the wave setup. (b) The cross section of the basin.

momentum balance according to *Longuet-Higgins and Stewart* [1964] is

$$\frac{dS_{xx}}{dx} + \rho g(h + \zeta) \frac{d\zeta}{dx} = 0. \quad (24)$$

[34] The analytical solutions of wave setup inside the surf zone and setdown outside the surf zone, based on linear wave theory, are

$$\zeta = -\frac{1}{2} \frac{a^2 k}{\sinh 2kh}, \quad (25)$$

$$\zeta(x) = \zeta_b + \frac{3\kappa^2/8}{1 + 3\kappa^2/8} [h_b - h(x)], \quad (26)$$

where ζ is the water elevation, a is the wave amplitude, k is the wave number, h is the water depth, h_b is the water depth at the breaker line, κ is the breaking index.

[35] To test the three RS formulations (M08, X04, and LHS) using CH3D-SWAN and the analytical solution, a simple test case is designed: the basin is 150 m by 150 m; the bottom slope of the bottom is 1:40, with 2.1 m depth in the flat bottom part and 0.1 m in the shallowest part. The cross section of the basin is shown in Figure 3b. The incident wave height is 0.6 m; the wave period is 5 s.

[36] The grid resolution is 10 m by 10 m in the horizontal with directions 16 vertical layers; the bottom roughness is

$z_0 = 0.4$; the breaking index is selected as $\kappa = 0.78$, which is the default value in SWAN. The wave setup from the numerical simulation and the analytical solution are shown in Figure 3a, which suggests that the numerical results from the three methods do not have much difference, and all match well with the analytical solution. This is no surprise because the analytical solution is based on the vertically integrated momentum equation.

3.2. The Undertow Test by *Ting and Kirby* [1994]: TK94

[37] The undertow, which is a near bottom compensating flow for mass transport and Stokes drift in the surf zone, was first studied by *Bagnold* [1940]. Many laboratory experiments have been done to measure the undertow over sloped bottom [e.g., *Hansen and Svendsen*, 1984; *Stive and Wind*, 1986; *Okayasu et al.*, 1988; *Ting and Kirby*, 1994].

[38] While some [e.g., *Svendsen*, 1984b; *Stive and Wind*, 1986; *Putrevu and Svendsen*, 1993] used theoretical methods to predict the undertow, others used numerical models. *Svendsen et al.* [2003] used two wave models and the quasi 3-D model SHORECIRC [*Dongeren et al.*, 1994] to simulate the wave-induced currents, and compared model results with measured data. *Christensen* [2006] conducted a large eddy simulation to study the turbulence and undertow induced by spilling and plunging breakers, while the undertow was successfully simulated, the simulated turbulence differed considerably with the observations. *Wang et al.* [2008] derived new expressions of vertically integrated

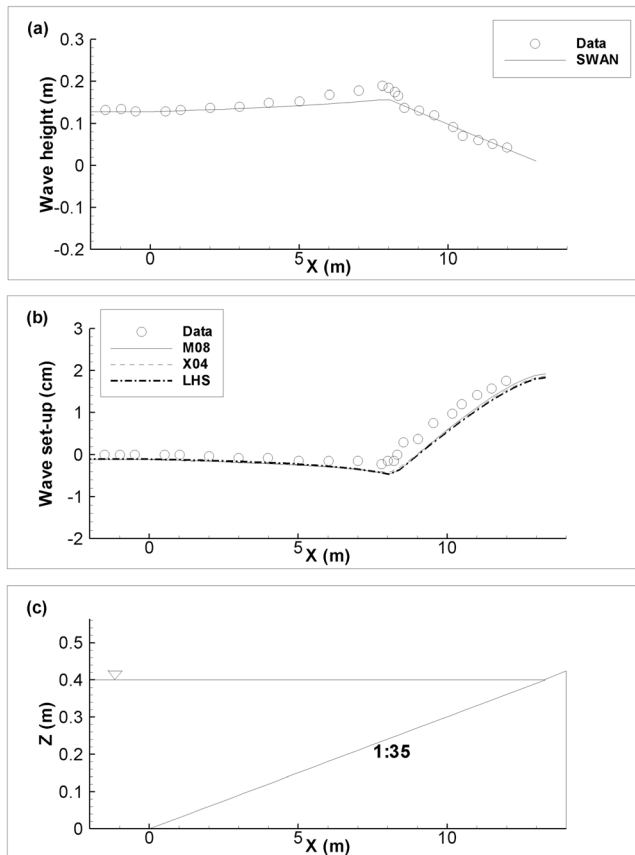


Figure 4. Comparison between the data and numerical results for (a) wave height and (b) wave setup. (c) The cross section of the basin.

radiation stress and volume flux based on nonlinear wave theory, and used the Boussinesq-type nonlinear wave model COULWAVE [Lynett and Liu, 2004] to simulate the currents induced by waves over a sloped bottom.

[39] With the recently developed depth-dependent radiation stress formulations, a fully 3-D simulation of the undertow is now possible by coupling a 3-D circulation model and a wave model. In this study, TK94 is simulated using the CH3D-SWAN modeling system and the depth-dependent radiation stress formulations, X04 and M08. The experiment was conducted in a two-dimensional wave tank, 40 m long, 0.6 m wide and 1.0 m deep, as shown in Figure 4c. The bottom slope is 1:35, and the water depth in the horizontal region is 0.4 m. The experimental data obtained with a wave height of 0.128 m in the horizontal region and a wave period of 5 s was simulated.

[40] The locations of measurements and water depths are shown in Table 1, where x is the horizontal distance in the wave tank, h is the local mean water depth, d is the local still water depth. In the experiment, the wave breaks at the location $x = 7.795$ m, which is station 2, so station 1 is outside the surf zone, and stations 3–7 are inside the surf zone.

[41] For the CH3D-SWAN simulations, the horizontal grid spacing is 35 cm, with 16 vertical layers. The simulation period is 15 min with a 0.005 s time step, until the simulation reaches the steady state. The flooding-drying feature is activated in CH3D, which allows water to occupy

the land cells. A variable vertical eddy viscosity as described by Sheng *et al.* [2010a] and a variable bottom friction coefficient with a bottom roughness $z_0 = 0.4$ are applied. The wave enhanced vertical eddy viscosity includes the vertical eddy viscosity calculated by the turbulence closure model [Sheng and Villaret, 1989] contained in CH3D, plus a wave-induced eddy viscosity following Battjes [1975]. The wave-enhanced bottom friction is calculated using the modified Grant and Madsen [1979] formula.

3.2.1. Wave-Induced Setup

[42] The wave height calculated by SWAN and the measured data are compared in Figure 4a, which shows good agreement. The simulated wave setup and the observed data as shown in Figure 4b, also agree well.

3.2.2. Wave-Induced Currents

[43] The CH3D-SWAN modeling system produces vertically varying wave-induced currents with all three RS formulations, as shown in Figure 5. These results show that quite different wave-induced flow patterns are produced by three different radiation stress formulations. Overall, M08 produces the best agreement with data, while X04 produces the worst agreement. Surprisingly, LHS, which is a depth-independent formulation, produces results that are better than those produced by X04, most likely because of the errors in X04. While the observed data reveal very abrupt vertical variation of the horizontal currents at ~ 0.25 – 0.35 of the water depth, the model results show gradual vertical variation of horizontal currents.

[44] Figure 6 shows that X04 produces one large clockwise gyre covering much of the wave tank. LHS produces a smaller clockwise gyre with little flow outside the surf zone due to weaker RS there. X04 produces two gyres: one stronger clockwise gyre with stronger flow at depths, plus a smaller counterclockwise gyre inside the surf zone. The simulated currents inside the surf zone have opposite direction to the observations, and the simulated downwelling at the breaker line contradicts the observation at station 2. The seaward undertow near the bottom is not correctly simulated. The reversed flow pattern in the surf zone alters the direction of the bottom friction, and affects the force balance between the bottom friction, pressure gradient and radiation stress. These inaccuracies in the X04 results apparently arise from the simplifications in the X04 formulation which assume small amplitude wave with respect to the local depth and wavelength. These simplifications render X04 invalid inside the shallow water region and the surf zone.

[45] The relative RMS errors of simulated results as calculated by equation (27) are shown in Table 2

$$\text{relative RMS error} = \frac{\sqrt{\frac{1}{N} \left[\left(\sum (x_{\text{model}}^i - x_{\text{data}}^i)^2 \right) \right]}}{\max(x_{\text{data}}^i)}, \quad (27)$$

Table 1. Locations of Measurements and Water Depths

	Stations						
	1	2	3	4	5	6	7
x (m)	7.295	7.795	8.345	8.795	9.295	9.795	10.395
d (m)	0.169	0.156	0.142	0.128	0.113	0.096	0.079
h (m)	0.166	0.154	0.143	0.132	0.119	0.104	0.090

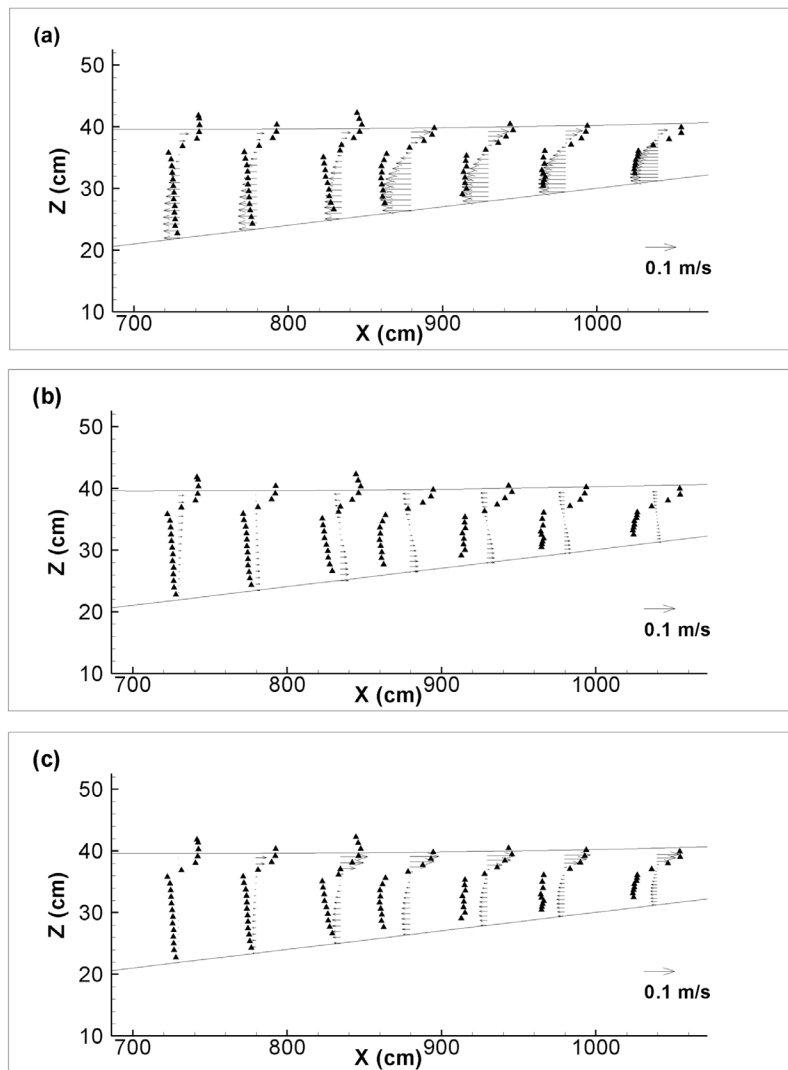


Figure 5. Comparison between the simulated (arrows) and measured (triangles) current velocities by using (a) M08, (b) X04, and (c) LHS radiation stresses. Stations 1–7 are given from left to right.

where x_{model} and x_{data} are simulated and observed results, respectively.

[46] As shown in Table 2, simulated mean currents (with Stokes drift subtracted) obtained using M08 are the best (26.2% error), while those obtained using X04 (82.6% error) are the worst. The flow direction obtained by using LHS is consistent with the observation in the surf zone. However, outside the surf zone, the simulated currents are negligible but incorrect (compared to station 1 data) due to relatively small radiation stress value resulting from uniform RS throughout the water column. The simulated upwelling at the breaker line does not agree with the observation at station 2.

[47] Using M08, the directions of the simulated currents are consistent with the observations. However, some discrepancies still exist between simulated currents and observations, possibly due to the following:

[48] 1. M08 is based on linear wave theory, and SWAN is a linear wave model. However, in the nearshore areas, especially in the surf zone, nonlinear process could play an important role.

[49] 2. The viscous effects of the boundary layer could be significant for the surf zone dynamics, but are not accounted for in the derivation of M08.

[50] 3. As indicated by TK94, different wave breakers may generate different mean flows. However, in the coupled CH3D-SWAN modeling system, the parameterization of different wave breakers has not been included.

[51] 4. Turbulence generated by breaking waves is important in determining the mean flow in the surf zone. Discrepancy between simulated and measured turbulent kinetic energy, to be discussed in section 3.2.3, apparently contributed to the errors in the simulated wave-induced currents.

[52] 5. The laboratory data may contain error due to such factors as wave reflections.

3.2.3. Turbulent Kinetic Energy

[53] The simulated turbulent kinetic energy (TKE) is compared to observations in Figure 7. To understand the relationship between the TKE and different RS formulations, the following explanation is given. Basically, the RS formulation affects the mean (wave averaged) currents

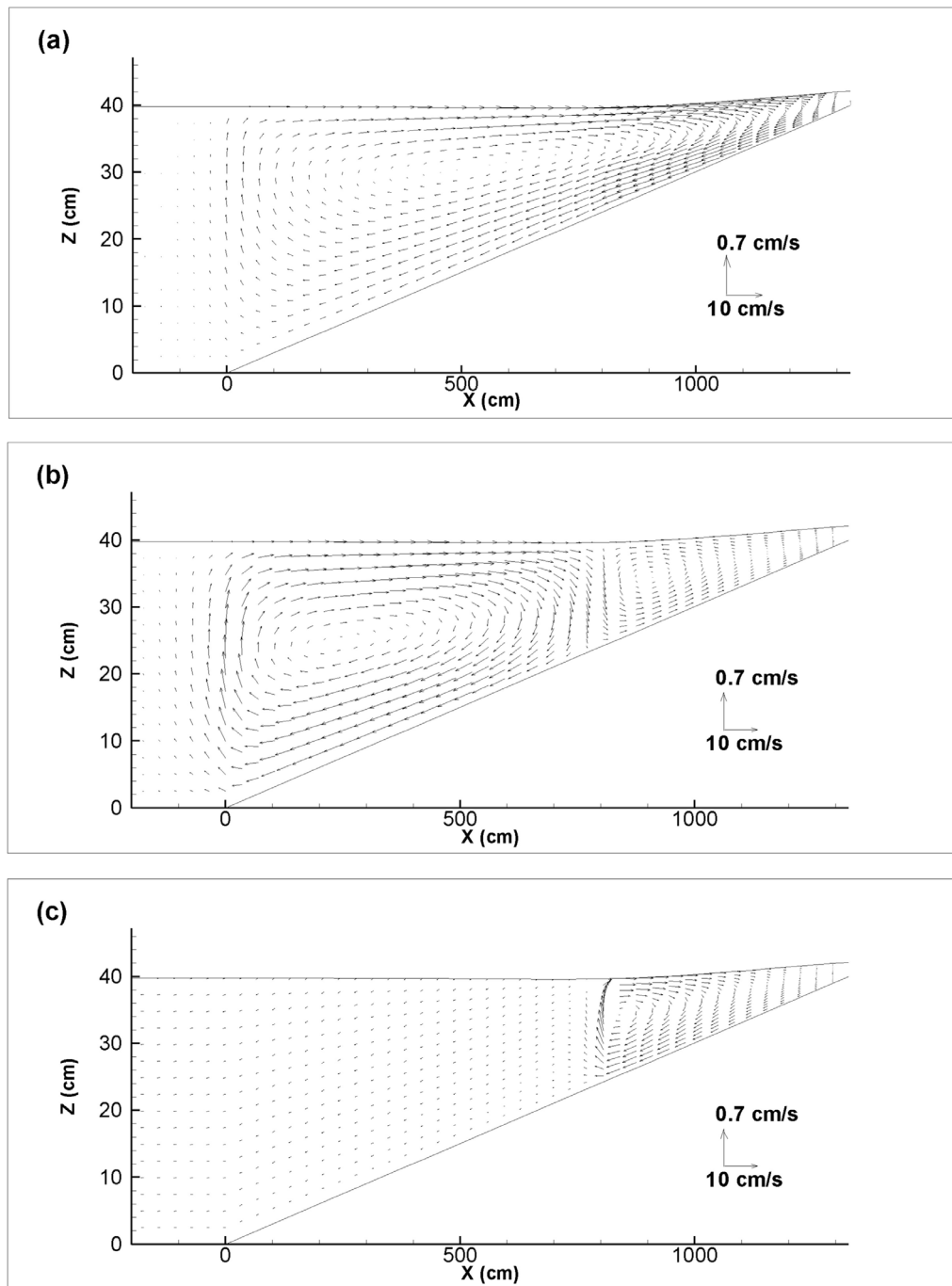


Figure 6. Wave-induced currents simulated by using (a) M08, (b) X04, and (c) LHS radiation stresses.

which in turn affect the TKE and eddy coefficients, which will affect the mean currents at the next time step. Therefore, errors in RS will affect the accuracy of the mean currents, TKE, and eddy coefficients. In CH3D, TKE and eddy viscosity are calculated using the equilibrium turbulent closure model [Sheng and Villaret, 1989] from the vertical gradients of mean currents (with Stokes drift subtracted) and hence does not include any wave-induced turbulence. Wave-induced eddy viscosity [Battjes, 1975] is then added to the current-induced eddy viscosity. The eddy viscosity which includes current and wave effects are used to simulate the

mean currents at the next time step. Therefore, the various RS formulation affect the TKE value via its effect on the vertical profile of mean currents, hence the RS formulation, M08, which gives the most accurate mean current, gives the most accurate TKE results. The TKE values simulated by CH3D-SWAN-M08 agree better with the TKE data measured at all seven stations by TK94 than those simulated by *Mocke* [2001] using a vertical one-dimensional $k-\varepsilon$ model [Rodi, 1980] with a roller dissipation term D_r . *Mocke* [2001] generally overestimated the measured TKE, particularly near the free surface, and did not simulate the mean currents.

Table 2. The Relative RMS Error for the Simulated Current Velocities

	RMS Error (%)									
	M08			X04			LHS			SWAN Wave Height
	Wave Setup	Mean Current	TKE	Wave Setup	Mean Current	TKE	Wave Setup	Mean Current	TKE	
Station 1	–	45.2	–	–	61.4	–	–	56.6	–	–
Station 2	–	45.0	–	–	74.6	–	–	44.4	–	–
Station 3	–	32.8	14.7	–	107.8	6.8	–	55.4	24.2	–
Station 4	–	37.2	16.0	–	142.7	32.3	–	95.4	41.8	–
Station 5	–	19.0	13.0	–	111.7	24.1	–	60.9	27.4	–
Station 6	–	27.5	10.3	–	130.6	18.5	–	72.6	28.5	–
Station 7	–	37.0	8.4	–	104.9	21.7	–	72.4	30.5	–
Overall	13.4	26.2	10.1	13.7	82.6	19.9	14.8	51.5	26.8	9.41

[54] The wave enhanced turbulence contributed by the wave energy dissipation D_b and the roller energy dissipation D_r described in Appendix A of Sheng et al. [2010a] are both activated in the simulation. The wave breaking affects the

vertical eddy viscosity A_v as is shown by Sheng et al. [2010a] where the parameter M is selected to be 0.025 according to De Vriend and Stive [1987].

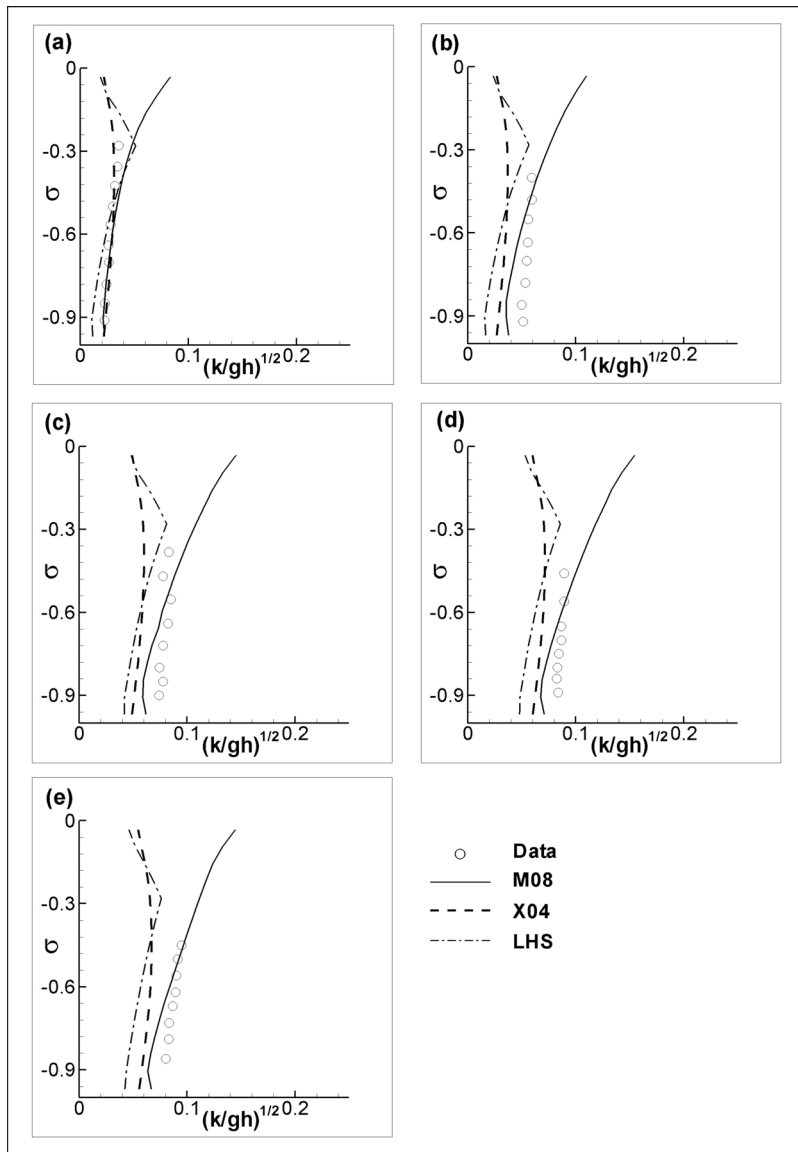


Figure 7. Comparison of turbulent kinetic energy between model results and data at (a) station 3, (b) station 4, (c) station 5, (d) station 6, and (e) station 7.

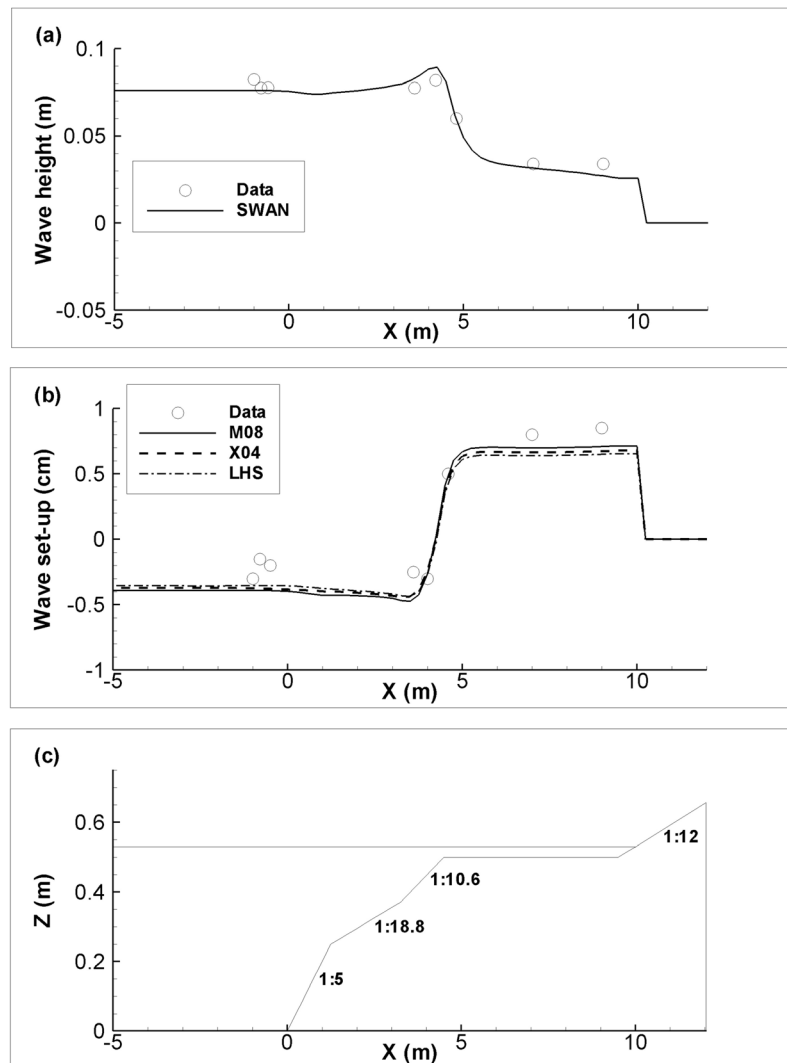


Figure 8. Comparison between the data and numerical results for (a) wave height and (b) wave setup. (c) The cross section of the basin.

[55] The relative RMS errors of the simulated TKE are shown in Table 2, which indicates that the depth-dependent radiation stress (M08, X04) gives more accurate results of TKE than the LHS radiation stress.

[56] While discrepancy between simulated and measured TKE can result from inaccuracy in the simulated mean currents, errors in simulated TKE can lead to inaccuracies in mean currents. To further verify and improve the TKE and mean currents simulation by CH3D-SWAN-M08, recent data of turbulence in the wave crest region [e.g., *Gemrich, 2010*] may be used.

3.3. Wave Setup on a Fringing Reef

[57] One of the three types of coral reefs, fringing reef grows fairly close to or directly from shore, with an entirely shallow lagoon or no lagoon at all. Fringing reefs are by far the most common reef type in the Greater Caribbean region and Red Sea. Fringing reefs also surround many South Pacific and Indian Ocean islands. Fringing reefs have a wide, shallow and flat bottom near the coastline, and drop into the deep water with a large slope. Wave often breaks at

the edge of the reef while propagating toward the coast, causing setup over the flat part. During hurricanes or typhoons, high waves and storm surge may cause damage and inundation over the relatively shallow area of the fringing reef.

[58] The study of wave setup over fringing reefs requires an accurate estimation of the wavefield over the reef by wave models, as well as the calculation of the setup and inundation by circulation models. Using the CH3D-SWAN modeling system, a fully 3-D simulation of the wave-induced setup and currents over a fringing reef is possible, and the accuracy of the model results can be evaluated by comparing with observations.

[59] In the laboratory experiment conducted by *Demirbilek et al. [2007]*, a 2-D fringing reef model was built in a 35 m long by 0.7 m wide wind-wave flume, where a series of experiments were conducted. A cross section of this reef-beach system is shown in Figure 8c. One experiment with an incident wave height of 0.075 m and a wave period of 1.5 s was selected.

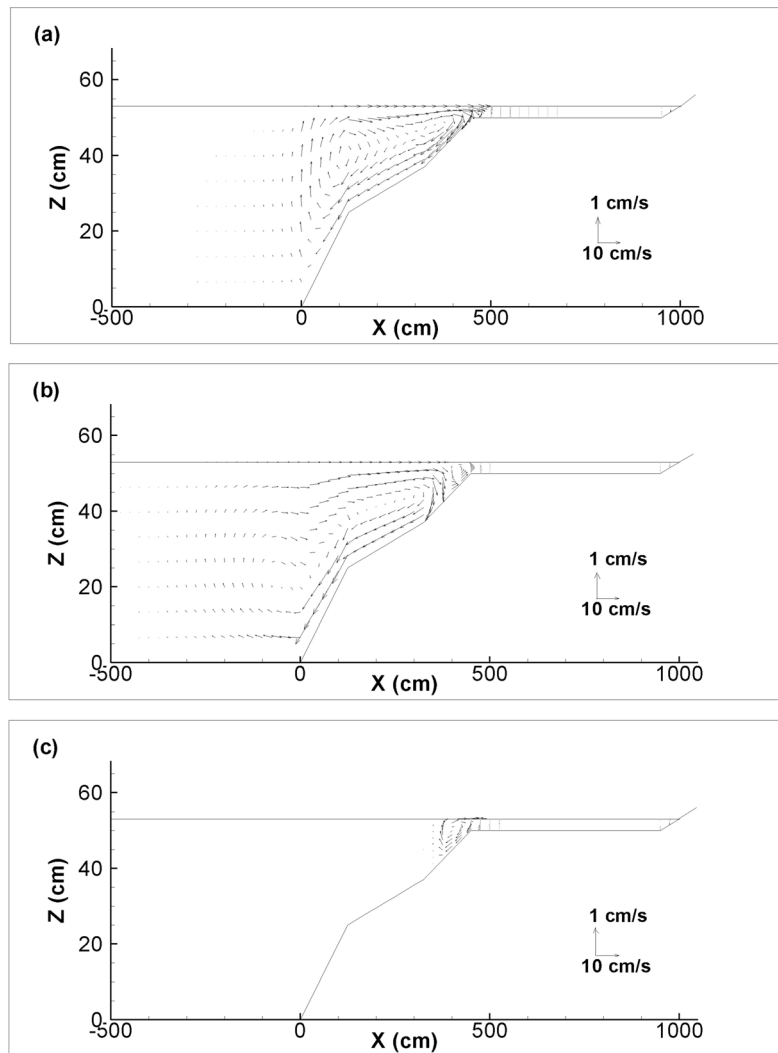


Figure 9. Wave-induced currents simulated by using (a) M08, (b) X04, and (c) LHS radiation stresses.

[60] The computational grid is 0.25 m by 0.25 m in the horizontal directions, and the water column is divided into 8 layers in the vertical direction. A vertically varying eddy viscosity with variable bottom friction, as well as the wave enhanced turbulent mixing [Battjes, 1975] and bottom friction with a bottom roughness $z_0 = 0.01$ are used in the simulation. The time step is 0.05 s, and the simulation is 30 min until the simulation reaches a steady state.

[61] The comparison between the wave height calculated by SWAN and the observations over the reef is shown in Figure 8a which shows good agreement. The comparison between the simulated and measured wave setup in Figure 8b also agrees well with each other.

[62] The simulated currents are shown in Figure 9. Although detailed measurements of the mean currents are not available for comparison and validation of the model results, comparison among model results are useful. The three flow patterns in Figure 9 all present a rather weak flow over the flat part of the reef. However, the mean flow patterns over the slope part are different: the currents from M08 show a shoreward flow at the surface and undertow near the

bottom; X04 produces a two gyre flow, while LHS radiation stress gives no currents outside the surf zone. The circulation gyre obtained with M08 agrees qualitatively with the flow trajectory recently observed by A. Sheremet et al. (unpublished manuscript, 2010). As mentioned in 3.2, the wave-induced currents simulated with X04 and LHS do not compare as well with the observed currents as those obtained with M08.

3.4. Simulation of Hurricane Isabel

[63] Sheng et al. [2010a] used LHS to simulate the storm surge, wave, and currents in the Outer Banks of North Carolina and Chesapeake Bay. In this study, LHS is replaced by the depth-dependent M08 in the CH3D-SSMS, and the model results are compared with data and previous results.

[64] The Isabel track and locations of all data stations are shown in Figure 10. The coastal domain as shown in Figure 10 has 548,240 grid cells. The 2-D vertically averaged version of ADCIRC [Luettich et al., 1992; Interagency Performance Evaluation Task Force, 2006] is used to

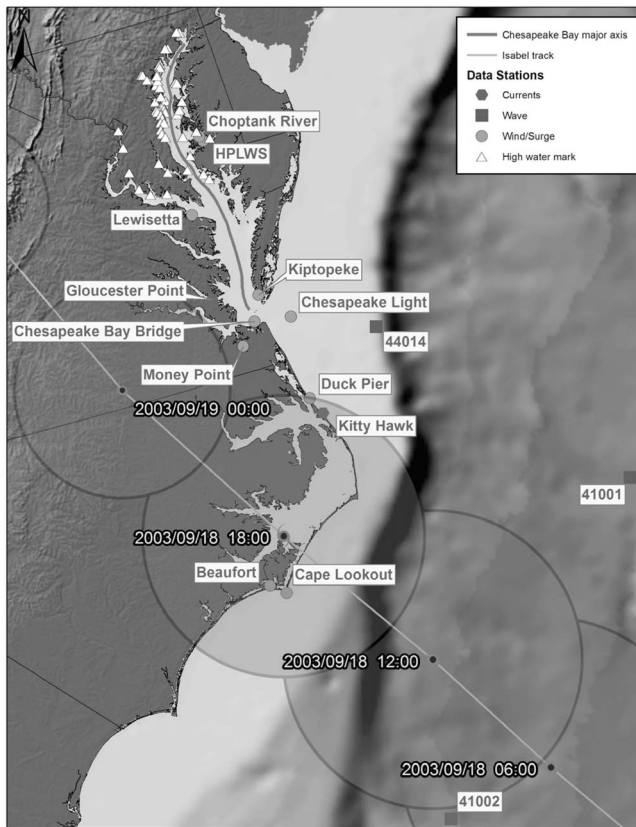


Figure 10. Isabel track showing locations of measured data and definition of the Chesapeake Bay major axis. Circles represent radiuses of maximum wind at each time.

simulate the regional/basin-scale surge over the entire Gulf of Mexico and western North Atlantic represented by the EC95d (ADCIRC Tidal Database, version ec_95d; see <http://www.unc.edu/ims/ccats/tides/tides.htm>) grid with 31,435 nodes, and to provide water elevation along the open boundaries of the coastal surge model CH3D. Tides along the CH3D open boundaries are provided by the ADCIRC tidal constituents [Mukai et al., 2002].

[65] The third generation wave model SWAN is used for wave simulation in the CH3D domain. Since Isabel traveled slowly, the stationary SWAN was applied. In the deep water, the model results of WAVEWATCH III (WW3) [Tolman, 1999] are used to provide the wave conditions along the open boundaries of the CH3D-SWAN domain. The domain of the WW3 model is similar to the ADCIRC domain. WW3 uses the WNA (western North Atlantic) wind, which is based on the GFDL (Geophysical Fluid Dynamics Lab) hurricane wind model.

[66] In this study, several wind models used by Sheng et al. [2010a] were applied: the WNA wind provided by National Centers for Environmental Prediction, the WindGen (WGN) wind provided through the University of Miami. The resolution of the WGN wind is 0.2° and the resolution of the WNA wind is 0.25° .

[67] The simulations used WGN or WNA wind, as well as the M08 radiation stress formulation to account for wave effects. The simulated water levels with WGN wind are compared with previous results and observations at two stations in Figure 11, which shows that the wave effects contribute significantly for the surge level. Without considering the wave effects, the surge level would be highly underestimated. However, the surge level simulated by M08 is only 1~3 cm higher than that simulated by LHS.

[68] The observed and simulated currents by using WNA wind at Kitty Hawk near the peak of the storm surge are shown in Figure 12. It is apparent that, using M08, the simulated currents are slightly improved over those obtained previously using LHS.

4. Conclusion

[69] In this study, a three-dimensional current-wave modeling system, CH3D-SWAN, has been enhanced with depth-dependent radiation stresses. This modeling system consists of a three-dimensional hydrodynamic model CH3D which is dynamically coupled to the model SWAN. Two depth-dependent (X04, M08) and one depth-independent (LHS) radiation stress formulations are considered, and their performances compared in this study.

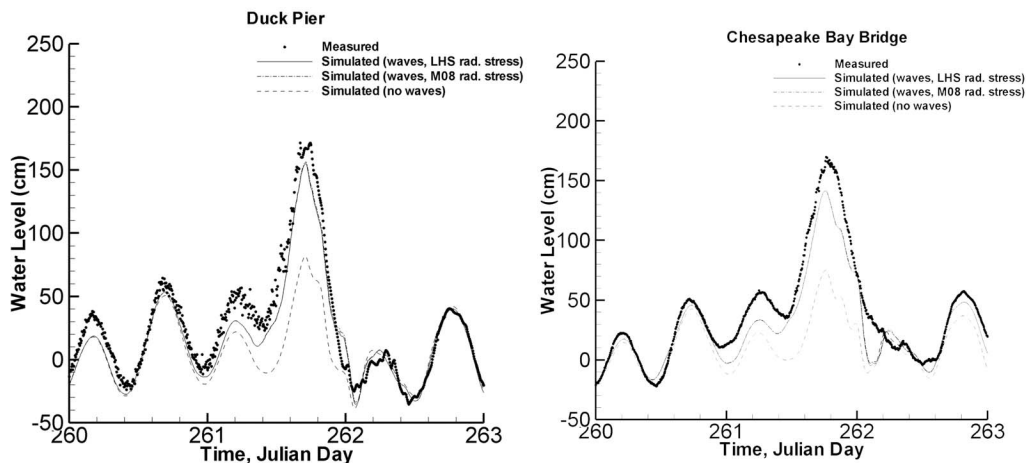


Figure 11. Measured and simulated water levels at two stations.

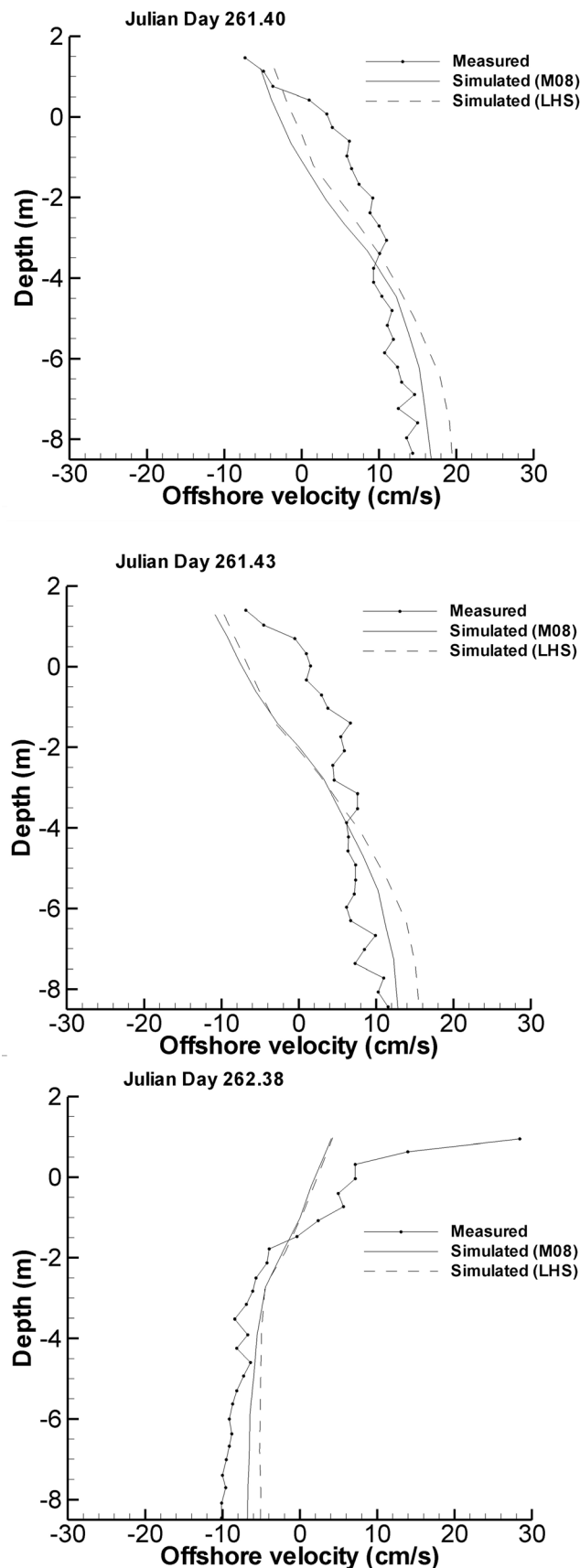


Figure 12. Measured and simulated onshore-offshore currents at Kitty Hawk during Isabel.

[70] Results of the coupled CH3D-SWAN compare well with analytical solution and laboratory observation of wave setup, and the three radiation stress formulations produce very slight difference in results. However, the different RS formulations produced noticeably different mean currents and turbulent kinetic energy.

[71] Wave-induced currents and turbulence observed during a laboratory undertow experiment (TK94) are also simulated, and the three different radiation stress formulations produce different mean flow patterns and turbulent kinetic energy. M08 gives the most accurate mean currents and turbulence, and the simulated currents have the correct direction inside and outside the surf zone. Using X04, the simulated currents inside the surf zone show a reversed flow pattern in comparison with the observations. LHS produces negligible flow outside the surf zone, which is inconsistent with the measured undertow. Discrepancy between the results obtained with M08 may be due to linear wave theory, the viscous effects of the boundary layer inside the surf zone, different breaker types not included in the model, and possible experimental errors. Further study is needed to more accurately predict the wave-induced currents in the nearshore area.

[72] The coupled modeling system using three RS formulations successfully simulates the wave height and wave setup over a laboratory model of a fringing reef. While the simulated wave setup is in agreement with the laboratory data, wave-induced currents over the fringing reef calculated by the coupled modeling system differs dramatically depending on the RS formulation used.

[73] Using the CH3D-SSMS and the M08 depth-dependent radiation stress formulation, storm surge and currents during Hurricane Isabel are also simulated. Waves contribute significantly to the surge level, and the depth-dependent radiation stress formulation produces similar storm surge but slightly improved currents which are driven by various processes (waves, wind, and tide), in comparison with data and previously obtained results using depth-independent LHS radiation stress formulation. This suggests that depth-dependent RS may not be needed for modeling storm surge and storm generated currents in a relatively mild storm such as Isabel. In stronger storms where wave effects may be more dominant, however, model results may show more noticeable differences.

[74] **Acknowledgments.** The authors would like to thank the support of Florida Sea Grant and NOAA IOOS program through a grant entitled A Regional Storm Surge and Inundation Model Testbed for the SECOORA Region. The authors also benefited from the valuable comments of two anonymous reviewers.

References

- Andrews, D. G., and M. E. McIntyre (1978), An exact theory of nonlinear waves on a Lagrangian-mean flow, *J. Fluid Mech.*, 89, 609–646, doi:10.1017/S0022112078002773.
- Arduin, F., N. Rasche, and K. A. Belibassakis (2008a), Explicit wave-averaged primitive equations using a generalized lagrangian mean, *Ocean Modell.*, 20, 35–60, doi:10.1016/j.ocemod.2007.07.001.
- Arduin, F., A. D. Jenkins, and K. A. Belibassakis (2008b), Comments on “The three-dimensional current and surface wave equations,” *J. Phys. Oceanogr.*, 38, 1340–1350, doi:10.1175/2007JPO3670.1.

- Bagnold, R. A. (1940), Beach formation by waves: Some model experiments in a wave tank, *J. Inst. Civ. Eng.*, 15, 27–52, doi:10.1680/ijoti.1940.14279.
- Battjes, J. A. (1972), Radiation stresses in short-crested waves, *J. Mar. Res.*, 30, 56–64.
- Battjes, J. A. (1975), A note on modeling of turbulence in the surf-zone, in *Symposium on Modeling Techniques*, pp. 1050–1061, Am. Soc. of Civ. Eng., Reston, Va.
- Booij, N., R. C. Ris, and L. H. Holthuijsen (1999), A third-generation wave model for coastal regions: 1. Model description and validation, *J. Geophys. Res.*, 104, 7649–7666, doi:10.1029/98JC02622.
- Christensen, E. A. (2006), Large eddy simulation of spilling and plunging breakers, *Coastal Eng.*, 53, 463–485, doi:10.1016/j.coastaleng.2005.11.001.
- Craik, A. D. D., and S. Leibovich (1976), A rational model for Langmuir circulation, *J. Fluid Mech.*, 73, 401–426, doi:10.1017/S0022112076001420.
- Demirbilek, Z., O. G. Nwogu, and D. L. Ward (2007), Laboratory study of wind effect on runup over fringing reefs, report 1: Data report, *Coastal Hydraul. Lab. Tech. Rep. ERDC/CHL-TR-07-4*, U.S. Army Eng. Res. and Dev. Cent., Vicksburg, Miss.
- De Vriend, D., and M. J. F. Stive (1987), Quasi-3D modeling of near-shore currents, *Coastal Eng.*, 11, 565–601, doi:10.1016/0378-3839(87)90027-5.
- Dongren, A. R., F. E. Sancho, I. A. Svendsen, and U. Putrevu (1994), SHORECIRC: A quasi 3-D nearshore model, in *Proceedings of the Twenty-Fourth International Conference*, edited by B. L. Edge, pp. 2741–2754, Am. Soc. of Civ. Eng., New York.
- Feddersen, F. (2004), Effect of wave directional spread on the radiation stress: Comparing theory and observations, *Coastal Eng.*, 51, 473–481, doi:10.1016/j.coastaleng.2004.05.008.
- Gemmrich, J. (2010), Strong turbulence in the wave crest region, *J. Phys. Oceanogr.*, 40, 583–595, doi:10.1175/2009JPO4179.1.
- Grant, W. D., and O. S. Madsen (1979), Combined wave and current interaction with a rough bottom, *J. Geophys. Res.*, 84, 1797–1808, doi:10.1029/JC084iC04p01797.
- Groeneweg, J. (1999), Wave-current interactions in a generalized Lagrangian mean formulation, Ph.D. thesis, Delft Univ. of Technology, Delft, Netherlands.
- Haas, K. A., and I. A. Svendsen (2000), Three-dimensional modeling of rip current system, *Res. Rep. CACR-00-06*, 250 pp., Cent. for Appl. Coastal Res., Univ. of Del., Newark, Del.
- Haas, K. A., and J. C. Warner (2009), Comparing a quasi-3D to a full 3D nearshore circulation model: SHORECIRC and ROMS, *Ocean Modell.*, 26, 91–103, doi:10.1016/j.ocemod.2008.09.003.
- Haas, K. A., I. A. Svendsen, M. C. Haller, and Q. Zhao (2003), Quasi-three-dimensional modeling of rip current systems, *J. Geophys. Res.*, 108(C7), 3217, doi:10.1029/2002JC001355.
- Hansen, J. B., and I. A. Svendsen (1984), A theoretical and experimental study of undertow, in *Nineteenth Coastal Engineering Conference: Proceedings of the International Conference*, edited by B. L. Edge, pp. 2246–2262, Am. Soc. of Civ. Eng., New York.
- Interagency Performance Evaluation Task Force (2006), Performance evaluation of the New Orleans and southeast Louisiana hurricane protection system, technical report, U.S. Army Corps of Eng., Vicksburg, Miss.
- Leonard, B. P. (1979), A stable and accurate convective modeling procedure based on quadratic upstream interpolation, *Comput. Methods Appl. Mech. Eng.*, 19, 59–98, doi:10.1016/0045-7825(79)90034-3.
- Leonard, B. P. (1991), The ultimate conservative difference scheme applied to unsteady one-dimensional advection, *Comput. Methods Appl. Mech. Eng.*, 88, 17–74, doi:10.1016/0045-7825(91)90232-U.
- Liu, H., and L. Xie (2009), A numerical study on the effects of wave-current-surge interactions on the height and propagation of sea surface waves in Charleston Harbor during Hurricane Hugo 1989, *Cont. Shelf Res.*, 29, 1454–1463, doi:10.1016/j.csr.2009.03.013.
- Longuet-Higgins, M. S. (1970a), Longshore currents generated by obliquely incident waves, 1, *J. Geophys. Res.*, 75, 6778–6789, doi:10.1029/JC075i033p06778.
- Longuet-Higgins, M. S. (1970b), Longshore currents generated by obliquely incident waves, 2, *J. Geophys. Res.*, 75, 6790–6801, doi:10.1029/JC075i033p06790.
- Longuet-Higgins, M. S., and R. W. Stewart (1962), Radiation stress and mass transport in gravity waves with application to “surf beats,” *J. Fluid Mech.*, 13, 481–504, doi:10.1017/S0022112062000877.
- Longuet-Higgins, M. S., and R. W. Stewart (1964), Radiation stresses in water waves; a physical discussion with applications, *Deep Sea Res.*, 11, 529–562.
- Luetlich, R., J. J. Westerink, and N. W. Scheffner (1992), ADCIRC: An advanced three-dimensional circulation model for shelves coasts and estuaries, report 1: Theory and methodology of ADCIRC-2DDI and ADCIRC-3DL, *Dredging Res. Program Tech. Rep. DRP-92-6*, U.S. Army Corps of Eng., Washington, D. C.
- Lynett, P., and P. L.-F. Liu (2004), A two-layer approach to water wave modeling, *Proc. R. Soc. London A*, 460, 2637–2669, doi:10.1098/rspa.2004.1305.
- McWilliams, J. C., J. M. Restrepo, and E. M. Lane (2004), An asymptotic theory for the interaction of waves and currents in coastal waters, *J. Fluid Mech.*, 511, 135–178, doi:10.1017/S0022112004009358.
- Mellor, G. L. (1996), *Users Guide for a Three Dimensional, Primitive Equation Numerical Ocean Model*, 39 pp., Princeton Univ. Press, Princeton, N. J.
- Mellor, G. L. (2003), The three-dimensional current and surface wave equations, *J. Phys. Oceanogr.*, 33, 1978–1989, doi:10.1175/1520-0485(2003)033<1978:TTCASW>2.0.CO;2.
- Mellor, G. L. (2008), The depth-dependent current and wave interaction equations; a revision, *J. Phys. Oceanogr.*, 38, 2587–2596, doi:10.1175/2008JPO3971.1.
- Mocke, G. P. (2001), Structure and modeling of surf zone turbulence due to wave breaking, *J. Geophys. Res.*, 106, 17,039–17,057, doi:10.1029/2000JC900163.
- Mukai, A. Y., J. J. Westerink, and R. A. Luetlich (2002), Guidelines for using the Eastcoast 2001 database of tidal constituents within the western North Atlantic Ocean, Gulf of Mexico and Caribbean Sea, *Coastal Hydraul. Eng. Tech. Note ERDC/CHL CHETN-IV-40*, U.S. Army Corps of Eng., Washington, D. C.
- Newberger, P. A., and J. S. Allen (2007), Forcing a three-dimensional, hydrostatic, primitive-equation model for application in the surf zone: 1. Formulation, *J. Geophys. Res.*, 112, C08018, doi:10.1029/2006JC003472.
- Okayasu, A., T. Shibayama, and K. Horikawa (1988), Vertical variation of undertow in the surf zone, paper presented at 21st International Conference on Coastal Engineering, Am. Soc. of Civ. Eng., Torremolinos, Spain.
- Putrevu, U., and I. A. Svendsen (1993), Vertical structure of the undertow outside the surf zone, *J. Geophys. Res.*, 98, 22,707–22,716, doi:10.1029/93JC02399.
- Rodi, W. (1980), *Turbulence Models and Their Application in Hydraulics—A State of the Art Review*, 104 pp., Assoc. for Hydraul. Res, Delft, Netherlands.
- Roland, A., A. Cucco, C. Ferrarin, T. Hsu, J. Liao, S. Ou, G. Umgiesser, and U. Zanke (2009), On the development and verification of a 2-D coupled wave-current model on unstructured meshes, *J. Mar. Syst.*, 78, S244–S254, doi:10.1016/j.jmarsys.2009.01.026.
- Sheng, Y. P. (1986), A three-dimensional numerical model of coastal and estuarine circulation and transport in generalized curvilinear grids, *Tech. Rep. 587*, 255 pp., Aeronaut. Res. Assoc. of Princeton, Princeton, N. J.
- Sheng, Y. P. (1987), On modeling three-dimensional estuarine and marine hydrodynamics, in *Three-Dimensional Models of Marine and Estuarine Dynamics, Elsevier Oceanogr. Ser.*, vol. 45, edited by J. C. J. Nihoul and B. M. Jamart, pp. 35–54, doi:10.1016/S0422-9894(08)70441-0, Elsevier, Amsterdam.
- Sheng, Y. P., and V. Alymov (2002), Coastal flooding analysis of Pinellas County using ALSM data: A comparison between UFs 2-D method and results vs. FEMA’s method and results, report, Dep. of Civ. and Coastal Eng., Univ. of Fla., Gainesville, Fla.
- Sheng, Y. P., and C. Villaret (1989), Modeling the effect of suspended sediment stratification on bottom exchange process, *J. Geophys. Res.*, 94, 14,429–14,444, doi:10.1029/JC094iC10p14429.
- Sheng, Y. P., V. Alymov, and V. A. Paramygin (2010a), Simulation of storm surge, wave, currents, and inundation in the Outer Banks and Chesapeake Bay during Hurricane Isabel in 2003: The importance of waves, *J. Geophys. Res.*, 115, C04008, doi:10.1029/2009JC005402.
- Sheng, Y. P., Y. Zhang, and V. A. Paramygin (2010b), Simulation of storm surge, wave, and inundation in the northeastern Gulf of Mexico during Hurricane Ivan in 2004, *Ocean Modell.*, 35, 314–331, doi:10.1016/j.ocemod.2010.09.004.
- Song, Y. T., and D. Haidvogel (1994), A semi-implicit ocean circulation model using a generalized topography following coordinate system, *J. Comput. Phys.*, 115, 228–244, doi:10.1006/jcph.1994.1189.
- Stive, M. J. F., and H. G. Wind (1986), Cross-shore mean flow in the surf zone, *Coastal Eng.*, 10, 325–340, doi:10.1016/0378-3839(86)90019-0.
- Svendsen, I. A. (1984a), Wave heights and set-up in a surf zone, *Coastal Eng.*, 8, 303–329, doi:10.1016/0378-3839(84)90028-0.
- Svendsen, I. A. (1984b), Mass flux and undertow in a surf zone, *Coastal Eng.*, 8, 347–365, doi:10.1016/0378-3839(84)90030-9.
- Svendsen, I. A., W. Qin, and B. A. Ebersole (2003), Modeling waves and currents at the LSTF and other laboratory facilities, *Coastal Eng.*, 50, 19–45, doi:10.1016/S0378-3839(03)00077-2.
- Ting, F. C. K., and J. T. Kirby (1994), Observation of undertow and turbulence in a laboratory surf zone, *Coastal Eng.*, 24, 51–80, doi:10.1016/0378-3839(94)90026-4.

- Tolman, H. L. (1999), User manual and system documentation of WAVEWATCH-III 1000 version 1.18, *OMB Tech. Note 167*, Natl. Cent. for Environ. Predict., Washington, D. C.
- Uchiyama, Y., J. C. McWilliams, and A. F. Shchepetkin (2010), Wave-current interaction in an oceanic circulation model with a vortex-force formalism: Application to the surf zone, *Ocean Modell.*, *34*, 16–35, doi:10.1016/j.ocemod.2010.04.002.
- Wang, B., A. J. Chadwick, and A. K. Otta (2008), Derivation and application of new equations for radiation stress and volume flux, *Coastal Eng.*, *55*, 302–318, doi:10.1016/j.coastaleng.2007.11.008.
- Xia, H., Z. Xia, and L. Zhu (2004), Vertical variation in radiation stress and wave-induced current, *Coastal Eng.*, *51*, 309–321, doi:10.1016/j.coastaleng.2004.03.003.
- Xie, L., K. Wu, L. Pietrafesa, and C. Zhang (2001), A numerical study of wave-current interaction through surface and bottom stresses: Wind-driven circulation in the South Atlantic Bight under uniform winds, *J. Geophys. Res.*, *106*, 16,841–16,855, doi:10.1029/2000JC000292.
- Xie, L., H. Liu, and M. Peng (2008), The effect of wave-current interactions on the storm surge and inundation in Charleston Harbor during Hurricane Hugo 1989, *Ocean Modell.*, *20*, 252–269, doi:10.1016/j.ocemod.2007.10.001.
- Zhang, M. Y., and Y. S. Li (1996), The synchronous coupling of a third-generation wave model and a two-dimensional storm surge model, *Ocean Eng.*, *23*, 533–543, doi:10.1016/0029-8018(95)00067-4.

T. Liu and Y. P. Sheng, Civil and Coastal Engineering Department, University of Florida, 365 Weil Hall, PO Box 116580, Gainesville, FL 32611-6580, USA. (pete@coastal.ufl.edu)